EDGE ARTICLE

Check for updates

Effective stabilization of a planar phosphorus(III) center embedded in a porphyrin-based fused aromatic skeleton†

Keisuke Fujimoto [iD] and Atsuhiro Osuka [iD]*

Organophosphorus(III) compounds usually take on stable pyramidal structures with a large inversion barrier of 30–35 kcal mol^{-1}. In contrast, diphenylphosphine-fused Ni(II) porphyrin, where the phosphorus atom is directly attached at the meso-position and embedded in a rigid skeleton, exhibits a considerably planarized phosphorus center. Here we report the synthesis of a mesityl-substituted Ni(II) porphyrin analogue, **6**, which allowed an evaluation of the inversion barrier ($\Delta G^{\ddagger}_{203}$) by variable temperature ^{1}H NMR spectroscopy which showed it to be exceptionally small, at 14.0 kcal mol^{-1}. The observed small inversion barrier has been attributed to conformational constraint imposed by the fused structure. In addition, it was thought that the planar transition state is stabilized by the Ni(II) porphyrin network that allows the contribution of a 22π-aromatic circuit involving phosphorus lone-pair electrons. Along this postulate, we attempted to engineer diarylphosphine-fused porphyrins with smaller inversion barriers by replacing the fused benzene rings with five-membered heterocyclic rings such as thiophene, benzothiophene, benzofuran, indole, benzothiophene 1,1-dioxide, and thiophene 1,1-dioxide. In that order, the aromatic character of the heterocycle decreases, which leads to increasing contribution of the 22π-aromatic circuit. Actually, the inversion barrier of the phosphorus center becomes smaller in this order and reaches 8.7 kcal mol^{-1} for thiophene 1,1-dioxide-fused Ni(II) porphyrin **15**, supporting the postulate.

Introduction

Organophosphorus(III) compounds usually take a stable pyramidal structure with a small inversion rate constant even at a high temperature ($k < 1.0 \times 10^{-3}$ s^{-1} at 130 °C) and a large activation barrier of the pyramidal inversion ($\Delta G^{\ddagger}$ = 30–35 kcal mol^{-1}).[1] The transition state in the pyramidal inversion is naturally considered to possess a planar phosphorus center. Thus, the inversion barrier may represent an energy difference between the pyramidal structure in the ground state and the planar structure in the transition state. Owing to the energetic disadvantage, planar phosphorus compounds have only been reported for extremely electron deficient cases such as cationic and carbene species.[2] While the pyramidal phosphorus(III) usually functions as a weak π-donor due to the intrinsic high *s*-character of the lone pair electrons,[3] the planarized phosphorus(III) compounds are expected to exhibit a considerable π-donating ability to cationic and carbene species. Intriguingly, computational studies also indicated that the inherent π-donating ability of an sp^2-hybridized planar phosphorus(III) atom was comparable to that of a nitrogen atom.[4] Hence, planar phosphorus(III) compounds are an attractive research target because of their structural novelty as well as their expected high electron-donating ability.

In the 1970s, Mislow *et al.* demonstrated that two approaches were effective to stabilize planar organophosphorus(III) compounds.[5] One approach was the attachment of electron-withdrawing groups at the phosphorus(III) atom as seen for silylphosphine[5a] and acylphosphine,[5b] which showed pyramidal inversion barriers ($\Delta G^{\ddagger}$) of 18.9 and 19.4 kcal mol^{-1}, respectively. The other approach was to incorporate lone-pair electrons of the phosphorus(III) atom into the $[4n + 2]\pi$ aromatic system. As a typical example, phospholes were reported to have remarkably small inversion barriers of 15–16 kcal mol^{-1},[5c] because the planar transition state efficiently interacted with neighboring π-units and attained a greater resonance (aromatic) stabilization energy than that in the pyramidal ground state.

Recently we reported a diphenylphosphine-fused Ni(II) porphyrin **1** that shows a considerably planar phosphorus center with a large CPC angle (sum of three CPC angles) of 322°.[6] While it looks natural to ascribe this planar P(III) center to the fused and constrained structure, similarly constrained

Department of Chemistry, Graduate School of Science, Kyoto University, Sakyo-ku, Kyoto, 606-8502, Japan. E-mail: osuka@kuchem.kyoto-u.ac.jp

organophosphorus(III) compounds such as methylene-, oxo-, and sulfur-bridged triarylphosphines **2–4** and phosphaperylene derivative **5** (Chart 1)[7] were reported to exhibit smaller CPC angles of 279–308° compared to that of triphenylphosphine (308°), indicating that the P(III) centers of **2–5** are fixed with more pyramidal conformations. Therefore, it was thought that, in addition to the structural constraint, the flexible electronic π-system of the Ni(II) porphyrin in **1** may be responsible for the observed planar P(III) center by allowing the contribution of the 22π-aromatic resonance that involves the lone-pair electrons of the P(III) center, similar to the case of phospholes. In this paper, we synthesized a mesityl-substituted diphenylphosphine-fused Ni(II) porphyrin **6** and its analogues, in which the mesityl groups can be used as labels in ^{1}H NMR spectroscopy for determination of the inversion barrier ($\Delta G^{\ddagger}$). Furthermore, the fused benzene rings were replaced by five-membered heterocycles with a variable degree of aromaticity to explore diarylphosphine-fused Ni(II) porphyrins with a smaller $\Delta G^{\ddagger}$ value.

Results and discussion

Synthesis of mesityl-substituted diphenylphosphine-fused porphyrin 6

Mesityl-substituted diphenylphosphine-fused porphyrin **6** was prepared by following the same procedure used in the synthesis of 3,5-di-*tert*-butylphenyl-substituted diphenylphosphine-fused porphyrin **1**(Scheme 1).[6] Mesityl-substituted 3,5,7-trichloro Ni(II) porphyrin **7** (ref. 8) underwent nucleophilic aromatic substitution with lithium diphenylphosphide and the subsequent oxidation with H_2O_2 gave 3,7-dichloro-5-diphenylphosphoryl-porphyrin **8**. Then, palladium-catalyzed intramolecular C–H arylation[9] of **8** afforded diphenylphosphine-oxide-fused porphyrin **9**, which was reduced with $HSiCl_3$ to provide **6**. The diphenylphosphine-fused porphyrin **6** could be stored as an air-stable solid without any special care, but was slowly oxidized in solution under ambient conditions.
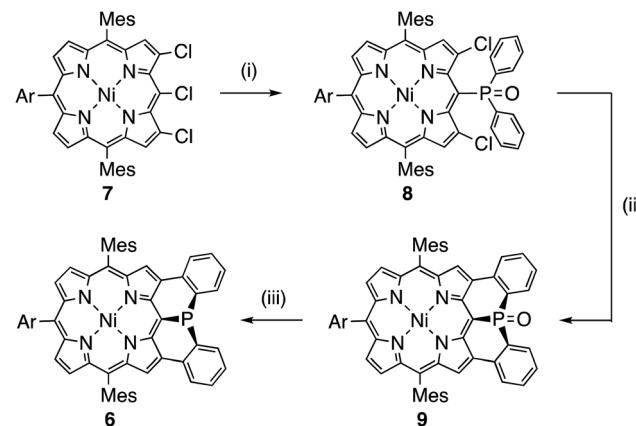
Scheme 1 Synthesis of diphenylphosphine-fused porphyrin **6** (Ar = 3,5-di-*tert*-butylphenyl). (i) LiPPh$_2$, THF, room temperature; then, H$_2$O$_2$, CH$_2$Cl$_2$, room temperature, 56%; (ii) Pd(OAc)$_2$, PCy$_3$·HBF$_4$, *t*BuCO$_2$H, K$_2$CO$_3$, *N*,*N*-dimethylacetamide, 120 °C, 46%; (iii) HSiCl$_3$, toluene, 110 °C, 65%.

X-ray crystallographic analysis of 6

The solid-state structure of **6** was revealed by X-ray crystallographic analysis (Fig. 1). Diphenylphosphine-fused Ni(II) porphyrin **6** formed a face-to-face dimer where the embedded phosphorus(III) atoms weakly coordinated to the central Ni(II) atoms in a complementary manner. Previously we reported that 3,5-di-*tert*-butylphenyl-substituted porphyrin **1** is diamagnetic in solution with a low-spin Ni(II) center but forms a paramagnetic face-to-face dimer with a five-coordinated Ni(II) center with a high-spin ($S = 1$) state in the solid state. As a characteristic structural feature of high-spin Ni(II) porphyrin, the Ni–N bond lengths of **1** are in the range of 2.026–2.038 Å, which are distinctly longer than those of low-spin Ni(II) porphyrins. While the dimeric structure of **6** is similar to that of **1**, the Ni–P bond length of 2.89 Å and interplanar distance of 4.00 Å are considerably longer than those (2.35 Å and 3.57 Å) of **1** due to steric congestion around the bulky mesityl groups. In addition, the Ni–N bonds (1.930–1.947 Å) are unchanged from those of usual low-spin, four-coordinated Ni(II) porphyrins. These structural
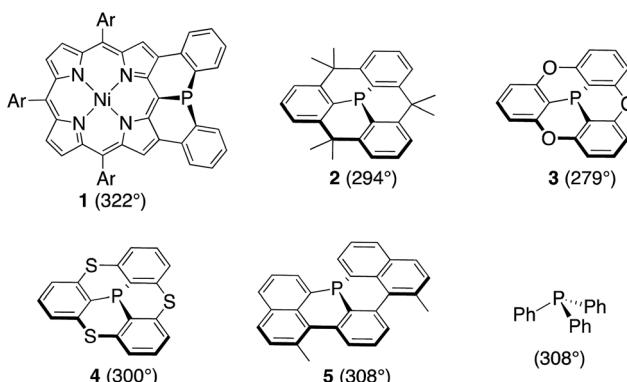
Chart 1 Structures and sum of three CPC angles of diphenylphosphine-fused Ni(II) porphyrin **1** (Ar = 3,5-di-*tert*-butylphenyl), phosphorus(III)-embedded π-conjugated molecules **2–5** and triphenylphosphine.
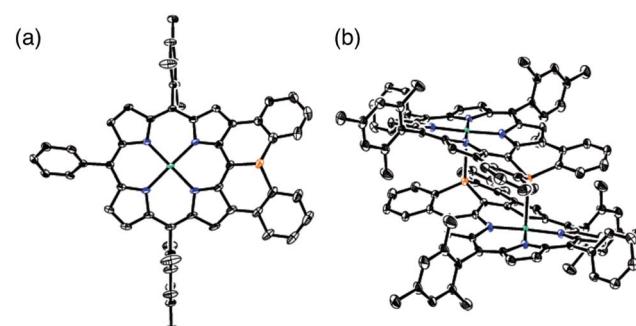

Fig. 1 X-ray crystal structures of **6** (a) top view and (b) packing structure. Solvent molecules, *tert*-butyl groups, and all hydrogen atoms are omitted for clarity. Thermal ellipsoids are drawn at the 50% probability level.

data indicate a low-spin state for the Ni(II) metal of **6** even in the solid-state. Actually, a temperature dependent magnetic susceptibility measurement showed a diamagnetic character for polycrystalline samples of **6** at 0.5 T from 2 to 300 K (see ESI, Fig. S117†).

Pyramidal inversion of the phosphorus center of 6

The inversion of the P(III) center of **6** was investigated by variable temperature ^{1}H NMR in CDCl$_3$ (Fig. 2). At -50 °C, **6** showed sharp signals at 2.46 and 1.25 ppm due to the methyl-protons H$_a$ and H$_b$, respectively, which became broader upon warming. These temperature-dependent spectral changes can be accounted for in terms of pyramidal inversion of the P(III) center.[10] The inversion rate constants k were determined at each temperature, from the full width at half maximum of the peak of H$_a$.[11] Then, a plot of the experimental $\ln(k/T)$ values *versus* $1/T$ was fitted into the Eyring equation using parameters of $\Delta H^{\ddagger} = 14.3$ kcal mol^{-1} and $\Delta S^{\ddagger} = 1.7$ cal (K^{-1} mol^{-1}). These values gave a pyramidal inversion barrier $\Delta G^{\ddagger}_{298} = 13.8$ kcal mol^{-1}, which is significantly smaller than those of normal phosphorus(III) compounds ($\Delta G^{\ddagger}_{403} = 30-35$ kcal mol^{-1}).[1] Namely, the planar transition state of **6** was significantly stabilized in this constrained molecular framework.

Theoretical study on 6′ and model compounds X and Y

To understand the observed small inversion barrier of the embedded phosphorus atom of **6**, we performed density functional theory (DFT) calculations on a simplified compound **6′** at the B3LYP/6-31G(d) level using the Gaussian 09 package (Fig. 3). A comparison of the total energies of the pyramidal ground state **A** and the planar transition state **B**[12] gave an inversion enthalpy of $\Delta H^{\ddagger} = 12.6$ kcal mol^{-1}, which was close to our experimental value for the Ni(II) complex **6** (14.3 kcal mol^{-1}). In addition, nucleus-independent chemical shift (NICS) calculations provided further insight into the aromaticity of **A** and **B** (Fig. 3b). The pyramidal structure **A** showed positive NICS(0) values at a (+4.37) and b (+2.97), indicating that an 18π aromatic circuit in the porphyrin core and two 6π aromatic circuits in the
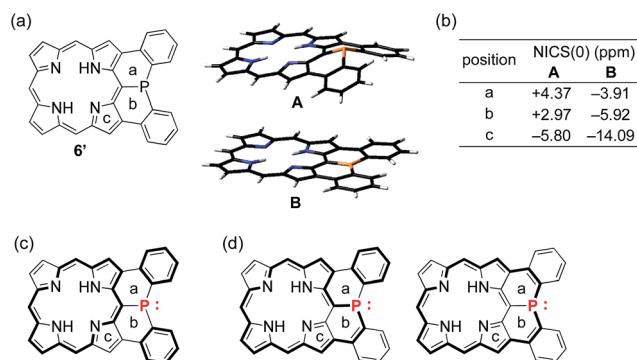
Fig. 3 (a) Structure of **6′**, pyramidal ground state **A** and planar transition state **B**, (b) NICS values of **6′**, (c) 18π aromatic circuit, and (d) 22π aromatic circuit involving the phosphorus lone-pair electrons. Points (a−c) are located at the centers of the six- or five-membered rings.

fused benzenes are dominant as drawn with bold lines (Fig. 3c). In contrast, the planar transition state **B** showed negatively shifted NICS(0) values at a (-3.91), b (-5.92), and c (-14.09), indicating a significant contribution of the 22π aromatic circuit passing through the planarized phosphorus atom (Fig. 3d). These results suggested that an effective π-conjugation through the planarized phosphorus atom enhances the 22π aromatic character to cause a greater aromatic stabilization in the planar transition state.

As demonstrated in annulene chemistry, the aromaticity of one annulene is perturbed by fusion of other aromatic rings and weakened to some degree.[13] The degree of the perturbation has a negative correlation with the double bond character of the fused bond which is shared with the parent annulene and the fused aromatic ring. For example, the inherent aromaticity tends to be retained by fusion of the 1–2 bond of naphthalene or the 2–3 bond of thiophene. On the other hand, prominent loss of the inherent aromaticity is induced by fusion of the 2–3 bond of naphthalene or the 3–4 bond of thiophene. This concept has been widely applied to modulate electronic properties of (anti) aromatic scaffolds, such as (dehydro)annulenes,[13] indacenes,[14] pentalenes,[15] and boroles.[16] Therefore, the strength of the above mentioned 22π aromaticity of the diphenylphosphine-fused porphyrin **6** should be controllable by replacing the fused benzene rings with other conjugated components. If the 22π aromaticity plays a crucial role in stabilizing the planar transition state, the enhancement of the 22π aromaticity provides more efficient stabilization of the planar phosphorus center. To verify this hypothesis, we initially conducted DFT calculations on bis(cyclopentadienyl)phosphine-fused porphyrin isomers **X** and **Y**, where the fused bonds of **6′** were replaced by double bonds and single bonds, respectively (Table 1). The calculations for **X** and **Y** were performed in a similar manner to the calculations for **6′**. The NICS calculation for **X** indicated a significant enhancement of the 22π aromaticity in the planar transition state with large negative NICS values at a (-10.15) and b (-11.99). In contrast, the calculation for **Y** showed a negligible contribution of the 22π aromatic circuit even in the planar transition state with positive NICS values at a (+3.67) and
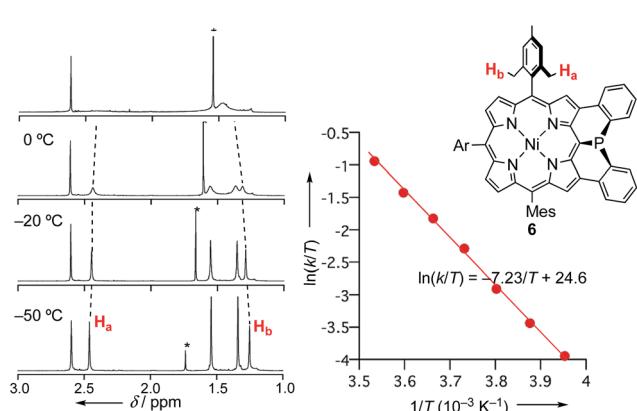
Fig. 2 Temperature-dependent ^{1}H NMR spectra of **6** in CDCl$_3$, and Eyring plot for determination of the pyramidal inversion barrier of the phosphorus center.

$\ln(k/T) = -7.23/T + 24.6$

Table 1 NICS(0) values (ppm) and relative energies (E_{rel}, kcal mol^{-1}) of model compounds **X** and **Y** in the pyramidal and planar structures
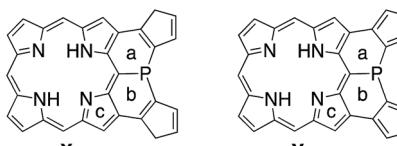
Compound (structure)	NICS(0) (ppm)			E_{rel} (kcal mol^{-1})
	a	b	c	
X (pyramidal)	+0.20	−1.12	−9.45	0
X (planar)	−10.15	−11.99	−17.71	7.8
Y (pyramidal)	+5.52	+5.59	−2.91	9.4
Y (planar)	+3.67	+3.62	−4.35	28.5

b (+3.62). Furthermore, calculated relative energies (E_{rel}) revealed that isomer **X** was more stable than **Y** by 9.4 kcal mol^{-1} in the pyramidal structure and 20.7 kcal mol^{-1} in the planar structure owing to the effective resonance (aromatic) stabilization. Thus, the calculated inversion barriers of **X** ($\Delta H^{\ddagger}$ = 7.8 kcal mol^{-1}) and **Y** ($\Delta H^{\ddagger}$ = 19.1 kcal mol^{-1}) were clearly correlated with the double bond character of the fused bonds and strength of the 22π aromaticites. The calculated pyramidal inversion barrier of **Y** is still smaller than that of normal phosphorus compounds due to the structural constraint on the phosphorus atom.

Synthesis of 10M and 11–15

Encouraged by the above consideration, we embarked on the synthesis of bis-heteroaromatic-fused porphyrins possessing thiophene (**10M**, M = Ni or Pd), benzothiophene (**11**), benzofuran (**12**), N-tosylindole (**13**), benzothiophene 1,1-dioxide (**14**), or thiophene 1,1-dioxide (**15**) with higher double bond character at the fused bonds (Schemes 2 and 3).[7d,f] Synthesis of **10M** and **11–15** has been achieved by developing a new synthetic route including a phospha-Friedel–Crafts reaction as a key step. First of all, a Negishi-coupling reaction of 3,7-diiodoporphyrin **16Ni**[8b] with the corresponding thienylzinc reagent under Pd-RuPhos catalysis[17] gave 3,7-di(5-methyl-2-thienyl)porphyrin **17Ni** in 86% yield. In the next step, incorporation of a phosphorus atom into this framework was attempted by a threefold phospha-Friedel–Crafts reaction. The reaction of **17Ni** with PBr$_3$ and ZnI$_2$ at 180 °C provided phosphine oxide **18Ni** in 54% yield after oxidation of the crude mixture with H$_2$O$_2$. In this reaction, ZnI$_2$ was employed as a moderate Lewis acid to accelerate the Friedel–Crafts reaction. Then, reduction of **18Ni** with HSiCl$_3$ gave dithienylphosphine-fused porphyrin **10Ni** successfully in 80% yield. Similarly to **6**, Ni(II) porphyrin **10Ni** formed an air-stable solid but was slowly oxidized in solution under ambient conditions. A palladium complex of dithienylphosphine-fused porphyrin **10Pd** was also synthesized from the 3,7-diiodoporphyrin palladium complex **16Pd** in three steps. Because the palladium complex **10Pd** was quite unstable

under air and oxidized immediately within a few seconds, the purification and spectroscopic analysis were conducted under strictly degassed conditions. Bis(benzothiophene)- and bis(benzofuran)-fused analogues **11** and **12** were also synthesized through a similar threefold phospha-Friedel–Crafts reaction, starting from 3,7-diiodoporphyrin **16Ni** in 36% and 42% yields respectively, in 3 steps. Compounds **11** and **12** were unstable toward air and gradually oxidized even in the solid-state.

Synthesis of di(N-tosylindolyl)phosphine-fused porphyrin **13** is also shown in Scheme 2. A Negishi-coupling reaction of **16Ni** with N-(phenylsulfonyl)indole and the subsequent deprotection of the sulfonyl group under strongly basic conditions gave 3,7-di(2-indolyl)porphyrin **24**. Then, a threefold phospha-Friedel–Crafts reaction with PBr$_3$ provided **25** in 81% yield without a Lewis acid owing to the high nucleophilicity of the indole parts. Then, N-tosylation and the subsequent reduction of the phosphine oxide furnished N-tosylindole-fused porphyrin **13** which was unstable under ambient conditions and gradually decomposed in both solution and solid state.

Synthesis of the di(thiophene 1,1-dioxide)-fused analogues **14** and **15** is shown in Scheme 3. The benzothiophene moieties of **20** were selectively oxidized with a tungsten-catalyst under biphasic conditions[18] to give the corresponding sulfone **27** in 84% yield. Then, reduction of **27** with HSiCl$_3$ proceeded selectively at the phosphine oxide part to give **14** in 26% yield. In a similar manner, di(thiophene)-fused **18Ni** was oxidized to sulfone **28** in 43% yield, and then reduced to the corresponding phosphine **15** in 28% yield. The structures of the intermediates **27** and **28** have been confirmed by X-ray diffraction analysis of their single crystals (see ESI, Fig. S101 and S102†). Compounds **14** and **15** were unstable toward air and gradually oxidized even in the solid-state, and more seriously they were quickly decomposed upon treatment with a silica-gel column, an alumina column, and a methanol solution. Therefore, pure compounds **14** and **15** were obtained through precipitation induced by addition of n-hexane into their CH$_2$Cl$_2$ solutions. In strictly degassed CD$_2$Cl$_2$ solutions, **14** and **15** were stable enough to allow the determination of the physical parameters of the phosphorus inversion discussed below.

Structural details of 6, 10M, and 11–15

The solid-state structures of **10Ni** and **12** were revealed by X-ray crystallographic analysis (Fig. 4).[19] Dithienylphosphine-fused Ni(II) porphyrin **10Ni** formed a face-to-face dimer involving complementary Ni–P coordination in the crystal (Fig. 4a and b). The Ni–P distance (2.92 Å), interplanar distance (4.02 Å), and Ni–N distances (1.931–1.948 Å) indicated that the packing structure of **10Ni** was almost the same as that of **6**.[7] In contrast, di(benzofuranyl)phosphine-fused porphyrin **12** formed a face-to-face dimer without a Ni–P bond. The dimerization was supported mainly by π-stacking interactions with a relatively large interplanar distance of 4.26 Å and parallel displacement of ca. 5 Å (Fig. 4c and d). The fused-benzofuran moiety formed a twisted [6]helicene-like structure due to a steric repulsion between two benzofuran units.
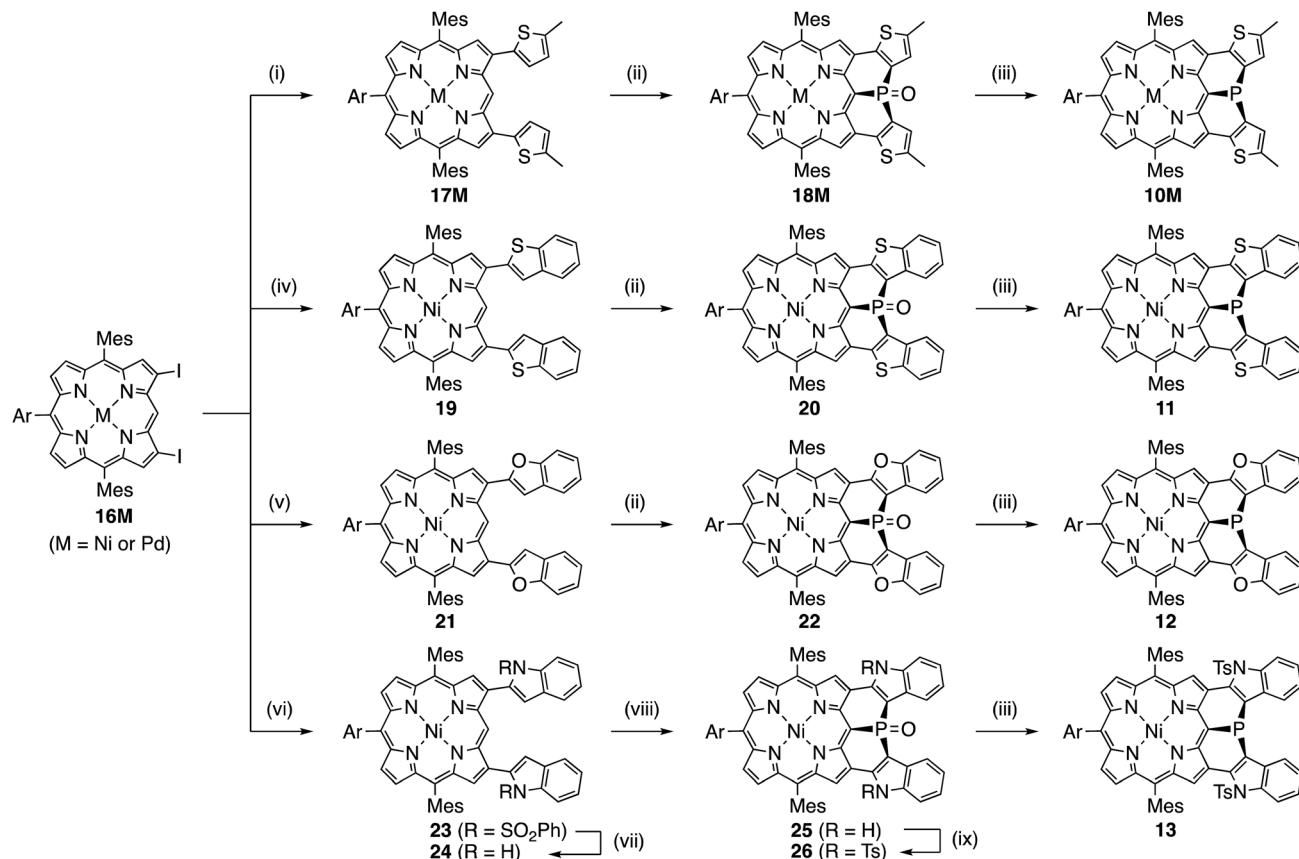
Scheme 2 Synthesis of diarylphosphine-fused porphyrins **10M** and **11–13** (Ar = 3,5-di-*tert*-butylphenyl). (i) 5-Methyl-2-thienylzinc chloride lithium chloride, Pd$_2$(dba)$_3$, ruphos, THF, reflux, (**17Ni**: 86%, **17Pd**: 91%); (ii) PBr$_3$, ZnI$_2$, *o*-dichlorobenzene, 180 °C; then, H$_2$O$_2$ (for **18Ni**, **20**, and **22**), (**18Ni**: 54%, **18Pd**: 53%, **20**: 59%, and **22**: 63%), (iii) HSiCl$_3$, toluene, room temperature, (**10Ni**: 80%, **11**: 69%, **12**: 81%, **13**: 26%), (iv) 2-ben-zothiophenylzinc chloride lithium chloride, Pd$_2$(dba)$_3$, ruphos, THF, reflux, 89%, (v) 2-benzofuranylzinc chloride lithium chloride, Pd$_2$(dba)$_3$, ruphos, THF, reflux, 83%, (vi) *N*-(phenylsulfonyl)-2-indolylzinc chloride lithium chloride, Pd$_2$(dba)$_3$, ruphos, THF, reflux, 67%; (vii) NaOH, THF/MeOH, reflux, 95%; (viii) PBr$_3$, *o*-dichlorobenzene, 180 °C, 81%; (ix) TsCl, CH$_2$Cl$_2$/NEt$_3$, reflux, 85%.
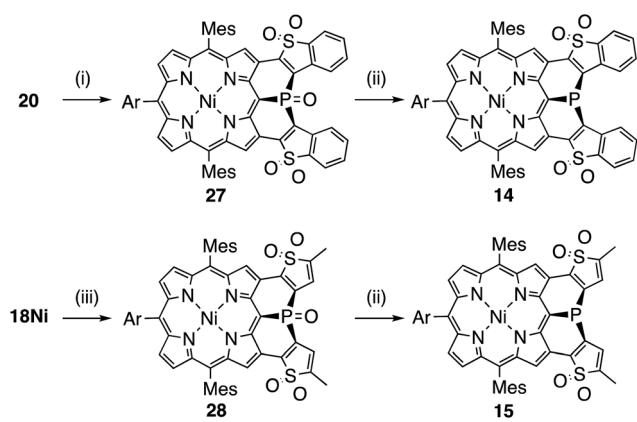
Scheme 3 Synthesis of (thiophene 1,1-dioxide)-fused porphyrins **14** and **15** (Ar = 3,5-di-*tert*-butylphenyl). (i) H$_2$O$_2$, Na$_2$WO$_4$·2H$_2$O, MeN(*n*-C$_8$H$_{17}$)$_3$·HSO$_4$, PhPO(OH)$_2$, toluene/H$_2$O, 50 °C, 84%; (ii) HSiCl$_3$, toluene, 110 °C, (**14**: 26%, **15**: 28%); (iii) H$_2$O$_2$, Na$_2$WO$_4$·2H$_2$O, MeN(*n*-C$_8$H$_{17}$)$_3$·HSO$_4$, PhPO(OH)$_2$, toluene/H$_2$O, 70 °C, 43%.

In addition to above mentioned X-ray crystal structures, DFT calculations were conducted to obtain the optimized structures of **6**, **10Ni**, **10Pd**, **11**, **12**, **14**, and **15** at the B3LYP/6-

31G*(C,H,N,O,P,S) + LANL2DZ(Ni,Pd) level using the Gaussian 09 package. The bond lengths and angles are summarized in Table 2. As discussed above, diarylphosphine-fused Ni(II) porphyrins tend to form a face-to-face dimer in the solid state, which causes structural deviations from the optimal confor-mations in solution. Hence, we will discuss the structural characteristics on the basis of the DFT calculated structures that are listed in Table 2. All compounds show significantly shorter P–C lengths than that of **PPh$_3$**. The bond shortening might be attributed to structural constraint due to the fused structure and more effective π-conjugation through the P(III) atom. Compounds **11**, **12**, and **14** showed different P–C2 and P–C3 lengths indicating a less symmetric structure caused by steric repulsion represented by short H1–H2 and C8–H2 distances. Compared to the fused benzofuran parts in **12**, the fused ben-zothiophene parts in **11** and **14** exhibited more steric conges-tion with shorter H2–C8 distances of 2.43 Å and 2.47 Å, respectively.

The planarity of the P(III) center has been evaluated from two factors. One is the sum of CPC angles, which gets closer to 360° with increased planarity. The other is the bottom depth, which gets closer to 0 Å with increased planarity. Compared to those of
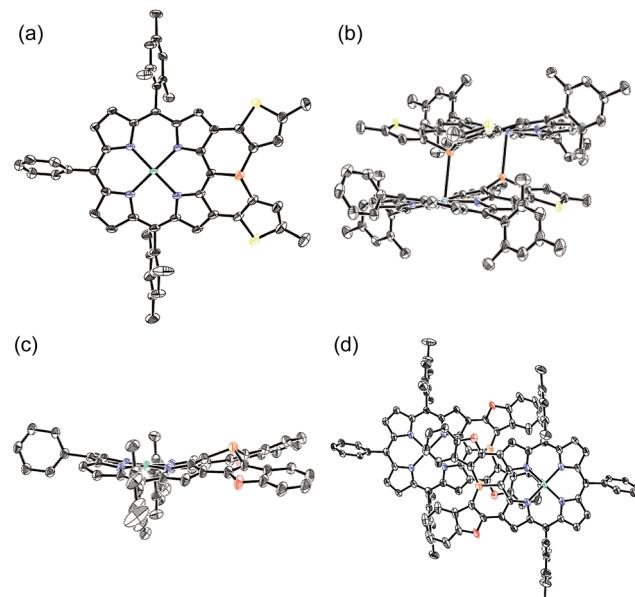
Fig. 4 X-ray crystal structures of **10Ni** and **12**. (a, b) Top view and packing structure of **10Ni**; (c, d) top view and packing structure of **12**. Solvent molecules, *tert*-butyl groups, and all hydrogen atoms are omitted for clarity. Thermal ellipsoids are drawn at the 50% probability level.

PPh₃ (307.8° and 0.81 Å), all diarylphosphine-fused porphyrins exhibit larger CPC angles (315.6–319.7°) and smaller bottom depths (0.68–0.72 Å), indicating that these P(III) centers take more planar structures. A comparison of **10Ni** and **10Pd** was used to evaluate the effect of the inner metal. In general, it is known that a Ni(II) porphyrin is relatively flexible to take a variety of non-planar structures such as ruffled and saddle-like

conformations, while Pd(II) porphyrin usually shows a rigid and planar structure.[20] The palladium complex **10Pd** showed a larger CPC angle and a smaller bottom depth, suggesting that the rigid Pd(II) porphyrin core holds the P(III) center into a more planar structure.

As the inherent double bond character of the fused rings increases in order of benzene < thiophene < benzothiophene < thiophene 1,1-dioxide, double bond characters of C2–C4 and C3–C5 are similarly increased in the order of **6** < **10Ni** and **10Pd** < **11** < **12** < **14** < **15**. Moreover, a similar tendency was observed in C4–C6 and C5–C7 bond lengths indicating the more effective π-conjugation between the porphyrin unit and the fused heterocycles.

Pyramidal inversion of P(III) centers

Pyramidal inversion of **10M** and **11–15** was investigated by variable temperature ¹H NMR measurements in CDCl₃ (for **10Ni** and **12–13**) or CD₂Cl₂ (for **10Pd**, **11**, and **14–15**) (Table 3). The activation enthalpy ($\Delta H^\ddagger$), entropy ($\Delta S^\ddagger$), and free energy ($\Delta G^\ddagger$) of **10M** and **11–13** were determined using Eyring plots in a similar manner to those of **6** as described above (see ESI, Fig. S108–S112†). Because the pyramidal inversion barriers of **14** and **15** were too small to be determined using Eyring plots, the activation free energies of **14** and **15** were estimated on the basis of their coalescence temperatures (see ESI, Fig. S113 and 114†).[11]

As compared with **6**, thiophene- and benzothiophene-fused porphyrins **10Ni** and **11** exhibited decreased inversion barriers of $\Delta G^\ddagger_{298} = 13.0$ kcal mol⁻¹ and $\Delta G^\ddagger_{298} = 12.2$ kcal mol⁻¹, respectively, because of the increased double bond character at the fused bonds. Benzofuran- and N-tosylindole-fused porphyrins **12** and **13** also showed smaller inversion barriers $\Delta G^\ddagger_{298} = 13.0$ kcal mol⁻¹ and $\Delta G^\ddagger_{298} = 13.4$ kcal mol⁻¹,

Table 2 Summary of the structural details of the diarylphosphine-fused porphyrins obtained from DFT calculation at the B3LYP/6-31G*(C,H,N,O,P,S) + LANL2DZ(Ni,Pd) level. All meso-substituents were replaced with phenyl groups to simplify the calculation

Compound	P–C1, P–C2, P–C3 (Å)	C2–C4, C3–C5 (Å)	C4–C6, C5–C7 (Å)	$\sum(\angle \text{CPC})$ (°)	Bottom depth (Å)	H1–H2 (Å)	H2–C8 (Å)
6	1.803, 1.835, 1.840	1.421, 1.422	1.461, 1.462	316.8	0.71	—	—
10Ni	1.813, 1.814, 1.814	1.387, 1.387	1.438, 1.438	315.6	0.72	—	—
10Pd	1.819, 1.811, 1.812	1.387, 1.387	1.438, 1.438	317.3	0.70	—	—
11	1.819, 1.818, 1.839	1.383, 1.385	1.436, 1.438	318.5	0.70	2.30	2.43
12	1.828, 1.805, 1.818	1.380, 1.381	1.426, 1.426	316.7	0.71	2.05	2.67
14	1.822, 1.818, 1.834	1.366, 1.368	1.424, 1.428	319.7	0.68	2.36	2.47
15	1.814, 1.808, 1.807	1.364, 1.364	1.425, 1.425	318.2	0.69	—	—
PPh₃	1.854	—	—	307.8	0.81	—	—

Table 3 Summary of activation enthalpy ($\Delta H^{\ddagger}$), entropy ($\Delta S^{\ddagger}$), and free energy ($\Delta G^{\ddagger}$) for phosphorus inversion of diarylphosphine-fused porphyrins

Compound	$\Delta H^{\ddagger}$ (kcal mol^{-1})	$\Delta S^{\ddagger}$ (cal (K^{-1} mol^{-1}))	$\Delta G^{\ddagger}_{298}$ (kcal mol^{-1})	$\Delta G^{\ddagger}_{203}$ (kcal mol^{-1})
6[a]	14.3	1.7	13.8	14.0
10Ni[a]	12.7	−0.9	13.0	12.9
10Pd[b]	10.2	−0.5	10.3	10.3
11[b]	9.1	−10.4	12.2	11.2
12[a]	12.0	−3.3	13.0	12.7
13[a]	12.8	−2.1	13.4	13.2
14[b]	—	—	—	9.2
15[b]	—	—	—	8.7

[a] In CDCl$_3$. [b] In CD$_2$Cl$_2$.

respectively. The inversion of **11** was entropically unfavorable ($\Delta S^{\ddagger} = -10.4$ cal (K^{-1} mol^{-1})) probably due to the steric congestion at the fused benzene rings. Compared to the nickel complex **10Ni**, the palladium complex **10Pd** showed a smaller inversion barrier of $\Delta G^{\ddagger}_{298} = 10.3$ kcal mol^{-1}, suggesting that the rigid palladium porphyrin skeleton more strictly enforced the phosphorus atom to stabilize the planar transition state. (Thiophene 1,1-dioxide)-fused porphyrins **14** and **15** displayed even smaller decreased inversion barriers of $\Delta G^{\ddagger}_{203} = 9.2$ kcal mol^{-1} and $\Delta G^{\ddagger}_{203} = 8.7$ kcal mol^{-1}, respectively. The observed stabilization of the planar transition state might be ascribed to an enhanced 22π-aromatic character of the porphyrin-including segment as well as the electron-withdrawing character of the sulfone groups.

Electronic properties

The UV/Vis absorption spectra of **6**, **10Ni**, and **11–15** in CH$_2$Cl$_2$ are shown in Fig. 5. Diphenylphosphine-fused porphyrin **6** exhibited a Soret band at 456 nm and Q bands at 564 and 610 nm, similar to the 3,5-di-*tert*-butylphenyl-substituted analogue **1**. Dithienylphosphine-fused **10Ni** provided a more perturbed spectrum with a broad and red-shifted Soret band at 457 nm and red-shifted Q band at 574 nm with a shoulder at

617 nm. Bis(benzothiophene)-, bis(dibenzofuran)-, and di(N-tosylindole)-fused **11–13** showed further red-shifted Soret bands at 468–473 nm and Q bands at 580–583 nm and 628–632 nm. The observed spectral red-shifts may be attributed to larger electronic interactions between the porphyrin unit and the fused heteroaromatic rings. Bis(1,1-dioxo-thienyl)phosphine-fused Ni(II) porphyrins **14** and **15** exhibited three split Soret bands around 350–550 nm and even more red shifted Q bands at 589–595 nm and 638–646 nm, probably reflecting the strongly electron-deficient fused heteroaromatics.

The redox potentials of **6**, **10Ni**, and **11–15** were measured by cyclic voltammetry or differential pulse voltammetry (Table 4, Fig. S115 and S116†). Compared to **6**, di(thienyl)phosphine-fused Ni(III) porphyrin **10Ni** displayed a slightly lower oxidation potential of 0.16 V and a higher reduction potential of −1.73 V. The resultant small electrochemical HOMO–LUMO gap (1.89 eV) of **10Ni** may be ascribed to more effective electronic perturbation by the fused thienyl units. On the other hand, bis(benzothienyl)phosphine-, bis(benzofuryl)phosphine-, and di(N-tosylindolyl)phosphine-fused Ni(II)porphyrins **11–13** showed positively shifted oxidation potentials in a range of 0.24 to 0.26 V and reduction potentials in a range of −1.66 to −1.70 V. Bis(1,1-dioxo-thienyl)phosphine-fused Ni(II) porphyrins **14** and **15** exhibited positively shifted oxidation potentials at 0.52 and 0.46 V, and reduction potentials at −1.40 and
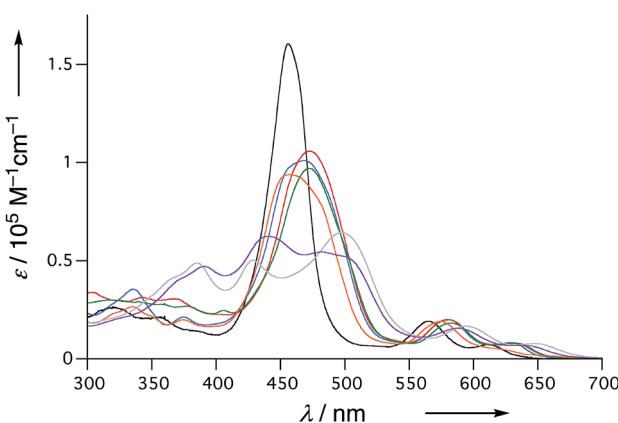
Fig. 5 UV/Vis absorption spectra of **6** (black), **10Ni** (orange), **11** (red), **12** (blue), **13** (green), **14** (gray), and **15** (violet) in CH$_2$Cl$_2$.

Table 4 Electrochemical potentials (V, *versus* ferrocene/ferrocenium ion couple) and HOMO–LUMO gaps (eV) measured in anhydrous CH$_2$Cl$_2$ with 0.1 M nBu$_4$NPF$_6$. Scan rate, 0.05 V s^{-1}; working electrode, glassy carbon; counter electrode, Pt wire; reference electrode, Ag/AgNO$_3$

Compound	E_{ox} (V)	E_{red} (V)	$\Delta E_{HOMO-LUMO}$ (eV)
6	0.21[a]	−1.76	1.97
10Ni	0.16[a]	−1.73	1.89
11	0.25[a]	−1.66	1.91
12	0.26[a]	−1.70	1.96
13	0.24[a]	−1.67[a]	1.91
14	0.52[a]	−1.40	1.92
15	0.46[a]	−1.37	1.83

[a] Irreversible, determined by DPV.

−1.37 V, respectively, because of the strongly electron-withdrawing nature of the oxidized heteroaromatic groups.

Conclusions

We synthesized mesityl-substituted diphenylphosphine-fused Ni(II) porphyrin **6**, in which the mesityl groups serve as a label in ^{1}H NMR spectroscopy for determination of the pyramidal inversion barrier of the P(III) center. Furthermore, a series of heterocycle-fused porphyrins **10M** and **11–15** were synthesized through a threefold phospha-Friedel–Crafts reaction as a key step to explore organophosphorus molecules with small pyramidal inversion barriers. Variable temperature ^{1}H NMR spectroscopy revealed exceptionally small inversion activation barriers of the P(III) centers of $\Delta G_{203}^{\ddagger} = 8.7–14.0$ kcal mol^{-1} for these fused porphyrins, indicating the efficient stabilization of the planar transition state. These results indicate that, in addition to the structural constraint due to the fused molecular frameworks, the effective aromatic stabilization of the planar transition state arising from the 22π-electronic circuit through a conjugative phosphorus center is responsible for the observed small inversion barriers.

Conflicts of interest

There are no conflicts to declare.

Acknowledgements

Notes and references

1 R. D. Baechler and K. Mislow, *J. Am. Chem. Soc.*, 1970, **92**, 3090.

2 (a) U. Heim, H. Pritzkow, H. Schönberg and H. Grützmacher, *J. Chem. Soc., Chem. Commun.*, 1993, 673; (b) C. Buron, H. Gornitzka, V. Romanenko and G. Bertrand, *Science*, 2000, **288**, 834.

3 (a) D. E. Cabelli, A. H. Cowley and M. S. Dewar, *J. Am. Chem. Soc.*, 1981, **103**, 3286; (b) J. C. Giordan, J. H. Moore, J. A. Tossell and W. Kaim, *J. Am. Chem. Soc.*, 1985, **107**, 5600.

4 (a) W. Kutzelnigg, *Angew. Chem., Int. Ed. Engl.*, 1984, **23**, 272; (b) J. K. Kapp, C. Schade, A. M. El-Nahasa and P. v. R. Schleyer, *Angew. Chem., Int. Ed. Engl.*, 1996, **35**, 2236.

5 (a) R. D. Baechler and K. Mislow, *J. Am. Chem. Soc.*, 1970, **92**, 4758; (b) W. Egan and K. Mislow, *J. Am. Chem. Soc.*, 1971, **93**, 1805; (c) W. Egan, R. Tang, G. Zon and K. Mislow, *J. Am. Chem. Soc.*, 1971, **93**, 6205.

6 (a) K. Fujimoto, Y. Kasuga, N. Fukui and A. Osuka, *Chem. –Eur. J.*, 2017, **23**, 6741; (b) N. Fukui, K. Fujimoto, H. Yorimitsu and A. Osuka, *Dalton Trans.*, 2017, **46**, 13322.

7 (a) D. Hellwinkel, A. Wiel, G. Sattler and B. Nuber, *Angew. Chem., Int. Ed. Engl.*, 1990, **29**, 689; (b) F. C. Krebs, P. S. Larsen, J. Larsen, C. S. Jacobsen, C. Boutton and N. Thorup, *J. Am. Chem. Soc.*, 1997, **119**, 1208; (c) G. K. H. Madsen, F. C. Krebs, B. Lebech and F. K. Larsen, *Chem. –Eur. J.*, 2000, **6**, 1797; (d) T. Hatakeyama, S. Hashimoto and M. Nakamura, *Org. Lett.*, 2011, **13**, 2130; (e) M. Yamamura, T. Saito and T. Nabeshima, *J. Am. Chem. Soc.*, 2014, **136**, 14299; (f) S. Hashimoto, S. Nakatsuka, M. Nakamura and T. Hatakeyama, *Angew. Chem., Int. Ed.*, 2014, **53**, 14074; (g) M. Yamamura, K. Sukegawa and T. Nabeshima, *Chem. Commun.*, 2015, **51**, 12080; (h) M. Yamamura, D. Hongo and T. Nabeshima, *Chem. Sci.*, 2015, **6**, 6373; (i) M. Yamamura and T. Nabeshima, *Bull. Chem. Soc. Jpn.*, 2016, **89**, 42; (j) M. Yamamura, T. Hasegawa and T. Nabeshima, *Org. Lett.*, 2016, **18**, 816.

8 (a) H. Hata, H. Shinokubo and A. Osuka, *J. Am. Chem. Soc.*, 2005, **127**, 8264; (b) K. Fujimoto, H. Yorimitsu and A. Osuka, *Org. Lett.*, 2014, **16**, 972; (c) N. Fukui, H. Yorimitsu and A. Osuka, *Angew. Chem., Int. Ed.*, 2015, **54**, 6311.

9 M. Lafrance and K. Fagnou, *J. Am. Chem. Soc.*, 2006, **128**, 16496.

10 Contribution of therotation of the mesityl groups is negligible at these temperatures(a) S. S. Eaton and G. R. Eaton, *J. Chem. Soc., Chem. Commun.*, 1974, 576; (b) S. S. Eaton and G. R. Eaton, *J. Am. Chem. Soc.*, 1975, **97**, 3660; (c) S. S. Eaton and G. R. Eaton, *J. Am. Chem. Soc.*, 1977, **99**, 6594; (d) C. J. Medforth, R. E. Haddad, C. M. Muzzi, N. R. Dooley, L. Jaquinod, D. C. Shyr, D. J. Nurco, M. M. Olmstead, K. M. Smith, J.-G. Ma and J. A. Shelnutt, *Inorg. Chem.*, 2003, **42**, 2227; (e) P. Wacker, K. Dahms, M. O. Senge and E. Kleinpeter, *J. Org. Chem.*, 2007, **72**, 6224.

11 F. P. Gasparro and N. H. Kolodny, *J. Chem. Educ.*, 1977, **54**, 258.

12 Optimization of **6′** with restriction to Cs symmetry provided the planar conformation **B** as the transition state. Frequency analysis of **B** showed one imaginary frequency corresponding to phosphorus inversion.

13 (a) T. C. Walsgrove and F. Sondheimer, *Tetrahedron Lett.*, 1978, **30**, 2719; (b) T. Nishinaga, H. Nakayama, N. Nobera and K. Komatsu, *Tetrahedron Lett.*, 1998, **39**, 7139; (c) R. H. Mitchell, *Chem. Rev.*, 2001, **101**, 1301; (d) A. J. Boydston, M. M. Haley, R. V. Williams and J. R. Armantrout, *J. Org. Chem.*, 2002, **67**, 8819; (e) E. Spitler, C. A. Johnson II and M. M. Haley, *Chem. Rev.*, 2006, **106**, 5344; (f) S. Kato, N. Takahashi, H. Tanaka, A. Kobayashi, T. Yoshihara, S. Tobita, T. Yamanobe, H. Uehara and Y. Nakamura, *Chem. –Eur. J.*, 2013, **19**, 12138.

14 (a) B. S. Young, D. T. Chase, J. L. Marshall, C. L. Vonnegut, L. N. Zakhariv and M. M. Haley, *Chem. Sci.*, 2014, **5**, 1008; (b) J. L. Marshall, K. Uchida, C. K. Frederickson, C. Schütt, A. M. Zeidell, K. P. Goetz, T. W. Finn, K. Jalolimek, L. N. Zakharov, C. Risko, R. Herges, O. D. Jurchescu and M. M. Haley, *Chem. Sci.*, 2016, **7**, 5547; (c)

C. K. Frederickson, L. N. Zakharov and M. M. Haley, *J. Am. Chem. Soc.*, 2016, **138**, 16827.

15 (*a*) T. Kawase, T. Fujiwara, C. Kitamura, A. Konishi, Y. Hirao, K. Matsumoto, H. Kurata, T. Kubo, S. Shinamura, H. Mori, E. Miyazaki and K. Takimiya, *Angew. Chem., Int. Ed.*, 2010, **49**, 7728; (*b*) H. Oshima, A. Fukazawa and S. Yamaguchi, *Angew. Chem., Int. Ed.*, 2017, **56**, 3270.

16 (*a*) A. Iida and S. Yamaguchi, *J. Am. Chem. Soc.*, 2011, **133**, 6952; (*b*) A. Iida, A. Sekioka and S. Yamaguchi, *Chem. Sci.*, 2012, **3**, 1461.

17 J. E. Milne and S. L. Buchwald, *J. Am. Soc. Brew. Chem.*, 2004, **126**, 13028.

18 K. Sato, M. Hyodo, M. Aoki, X.-Q. Zheng and R. Noyori, *Tetrahedron*, 2001, **57**, 2469.

19 The solid state structures of the phosphine oxides **18Ni**, **18Pd**, **20**, **22**, **26**, **27**, and **28** were revealed by X-ray crystallographic analysis (see ESI, Fig. S96–S102).†

20 *The Porphyrin Handbook*, ed. K. M. Kadish, K. M. Smith and R Guilard, Academic Press, USA, 2000, vol. 3.